Universiteit Utrecht

Age and origin of Megabeds in the Tabernas basin (Upper Miocene, SE Spain)

MSc thesis J.G. Koopmans
University Utrecht
2012

F.J. Hilgen (1st supervisor)
W. Krijgsman (2nd supervisor)

Abstract

The Tabernas basin in South-East Spain is an elongated intramontane basin of Neogene age and is part of the Internal Zone of the Betic Cordillera. Megabeds consisting of thick lithic mass-flow debris are found in dominantly turbiditic stratigraphy. The age of these megabeds has until now been unclear, hampering the understanding of their origin. By performing an integrated study on the Puente de Los Callejones section resulting in a detailed litho-, bio-, and magnetostratigraphy, we show that Megabed (MB) 1, 3 and the Gordo megabed (MB2/GMB) are of Late Tortonian age, while MB 4, 5, 6 and 7 are of Early Messinian age. Applying linear interpolation using calculated sedimentation rates yields megabed ages of: MB1) 7.411 ± 0.003; GMB) 7.375 ± 0.018; MB3) 7.358 ± 0.005; MB4) 7.060 ± 0.013; MB5) 7.031 ± 0.009; MB6) 6.963 ± 0.016; and MB7) 6.930 ± 0.022 Ma.

The boundary between Unit C and D (as defined by Haughton) is located at a stratigraphic level of 35.3 m in the section and has an age of 7.515 Ma.

The newly discovered MB6 and MB7 have a different, less lithic appearance and are together with MB4 and 5 exposed in a continuous ridge with clear difference in erosional profile, with megabeds located in more pronounced turbiditic sequences. We suggest that sediment overburden or availability of sediments is of importance for the deposition of megabeds, since the megabeds: 1) share a sheetlike deposition style; 2) are all single event mass-flows; 3) are more common in the stratigraphic record then previously thought; 4) the system supplying mass-flow material might have been active for a long time; 5) seem to coincide with periods of increased thickness (relief) and frequency of turbidites. The overburden or sediment availability might be linked to climate cyclicity.

Sedimentation rates in the Tabernas basin during the Late Tortonian to Early Messinian are an order of magnitude higher than in the adjacent Sorbas basin. The megabeds in the Tabernas basin cannot be linked to the Sorbas thick shell-debris (TSB) layers because of lacking age constraints, although we think a correlation is plausible.

We recommend to improve the biostratigraphic resolution of astronomically tuned sections by increasing the amount of accurate calibration points, such as the coiling changes of *Globorotalia scitula* and possible morphological variations. The enhanced resolution biostratigraphy is needed to more accurately date the megabeds located in high sedimentation rate environments in order to study the suggested cyclicity.

Keywords: Megabeds; Gordo; Tabernas; Tortonian; Messinian; Mediterranean; turbidites

studentnr: 3034534

Introduction

The Tabernas basin, located in South-East Spain (Fig. 1), contains us a unique and impressive sedimentary stratigraphic record expressing thick mass flow deposits with often large schistose blocks, termed megabeds. The megabeds, and in particular the thickest most widespread megabed called the Gordo Megabed, have sparked scientific interest for their implications on the basin itself as well as the associated processes causing them. The Gordo megabed has been thought to be triggered by a seismic event causing failure of either; 1) basin margins, 2) earlier uplifted basal breccias, 3) proximal parts of contemporary gravelly aprons (Kleverlaan, 1987; Haughton, 2000, 2001). The Gordo Megabed (GMB, MB2) has been studied most extensively while other megabeds are less clearly identified and described, creating possibilities for differences in their origin.

Thus far, the age of the megabeds has not been accurately established and the Tortonian/Messinian-boundary has not been pinpointed in the Tabernas basin (Haughton, 2000). Detailed study on the spacing between the megabeds and the relative and absolute ages of the stratigraphy and related sedimentation rates is needed to better understand the origin of these megabeds. This would enable us to better understand both the structural and sedimentary processes which have been active in the Tabernas basin, to enhance the comprehension of its history. Therefore, the aim of this study is to obtain more accurate ages for the megabeds, by precisely defining section localities and presenting a solid integrated stratigraphic (litho-, bio-, magneto-stratigraphic) framework for the megabeds.

For this purpose we selected the Puente de Los Callejones section, because it exposes the most continuous stratigraphy and has been studied before (albeit at a lower resolution) for stratigraphy below and up to the GMB (Haughton, 2000). Since the Tabernas area is complex, with many faults located in soft sediments, and most individual layers are not laterally traceable for long distances, the section consists of four subsections which can later be (partly) correlated (into a composite section). An integrated fieldwork was organized, planning to capture the lithostratigraphy, biostratigraphy and magnetostratigraphy of the stratigraphic interval covering the megabeds.

Geological setting and section

Basinal setting

The Sorbas-Tabernas basin is one of the intramontane basins of Neogene age (Iaccarino, 1975; Weijermars et al., 1985) that is part of the Internal Zone of the Betic Cordillera (Platt and Vissers, 1989). The Betic Cordillera has a basin-and-range-type morphology with elongated mountain ranges of mainly metamorphosed Paleozoic and Mesozoic lithologies, separated by narrow elongated basins (Platt and Vissers, 1989), one of them being the Sorbas-Tabernas basin. The basin was east-west orientated, with during the Late Miocene a deeper marine center of ca 600 m depth and dimensions of about 10 km width and several tens of kilometers length (Kleverlaan, 1989a; Haughton, 2000). The origin of the basins has been under extensive study and debate, with several modes of basin formation being proposed: (1) strike-slip (Montenat et al., 1987; Kleverlaan, 1989a; Poisson et al., 1999); (2) thrust-top (De Lamotte et al., 1995); and (3) extensional (Platt and Vissers, 1989; Vissers et al., 1995). Meijninger and Vissers (2006) state that a strike-slip origin of the basins is contradictionary with both recent structural studies of the underlying Betic basement and with the overall basin and fault geometry. They conclude that the Neogene basins developed as genuinely extensional basins, presumably associated with the thinning and exhumation of the underlying basement during the Late Miocene. However, when studying faults and deformation in the Tabernas basin itself, strike-slip syndepositional faulting is discussed to be the best fitting formation mode (Haughton, 2000; Hodgson and Haughton, 2004).

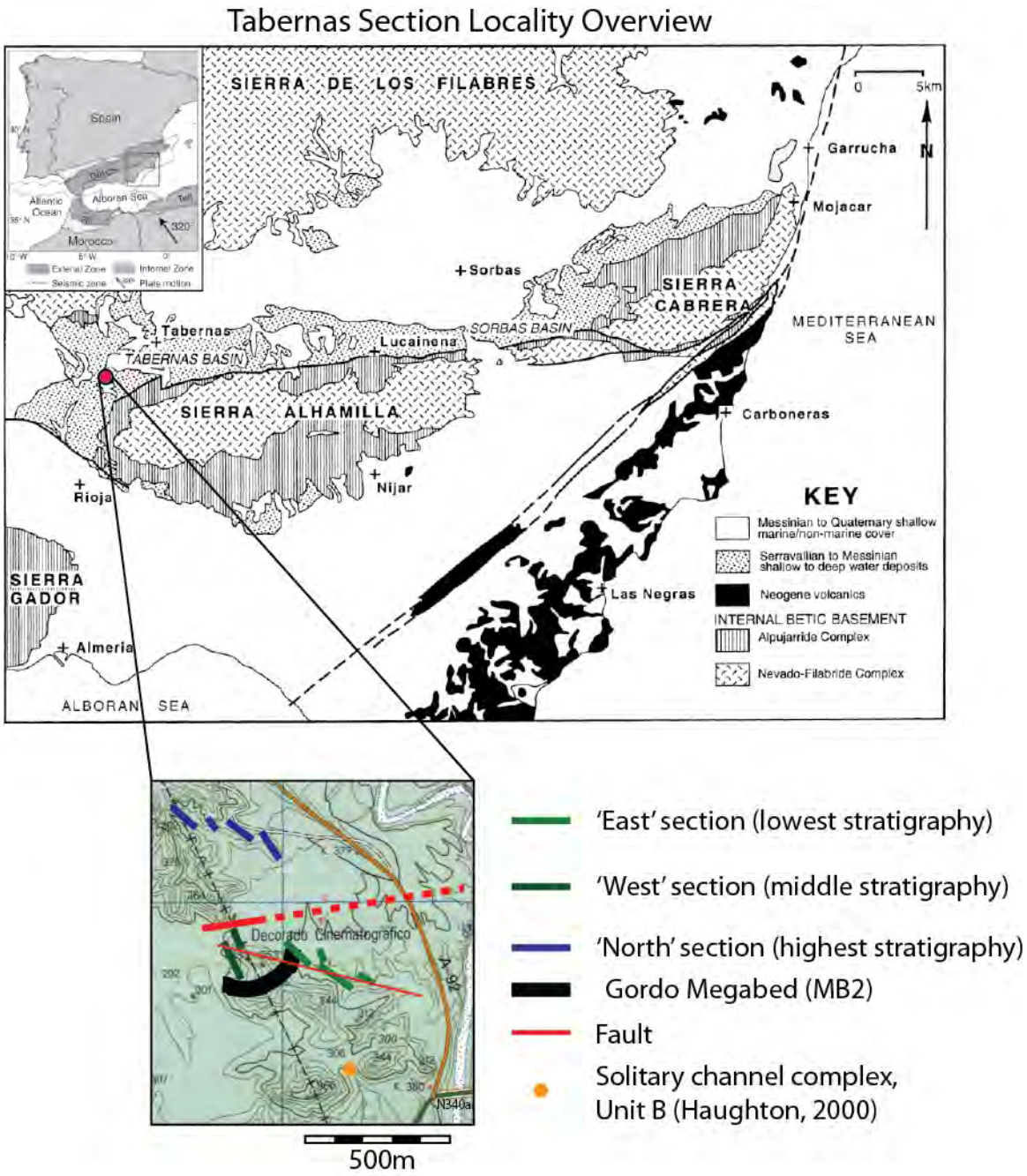

Figure 1. Overview of Tabernas basin and section locality. Overview map modified from Haughton (2000).

Stratigraphy

Sediment gravity flow deposits dominate the basin fill in the Tabernas basin during the Late Miocene. Tectonics played a key role in driving the evolution of the turbidite systems in the basin and deformation of the basin floor had an important impact on gradients, slope stability, bathymetry and the ability of flows to bypass along the trough axis (Haughton, 2000).

The Tabernas basin was interconnected with the Sorbas basin to the east, even though a structural high was likely in place between the two during the Late Tortonian to Early Messinian, preventing turbiditic sediments from the Tabernas basin to enter the Sorbas basin (Weijermars et al., 1985; Haughton, 2000). More specifically, Haughton (2000) suggests that from stratigraphic unit C (as defined in his paper) onwards, mainly consisting of thick grey bioturbated and slump-deformed marls, the Sorbas basin is uplifted causing sediment damming between the basins and shifting of the depocenter to the deeper Tabernas basin in

which subsidence was fault-controlled. Meanwhile the Sorbas basin was deformed, of which the Late Tortonian unconformity is an expression which is present in the Sorbas basin and eastern part of the Tabernas basin (Weijermars et al., 1985).

The stratigraphy of (West) Tabernas basin has been described previously (Weijermars et al., 1985; Kleverlaan, 1987, 1989a; Haughton, 2001) by a global succession of; 1) restricted red alluvial fan deposits positioned directly onto the alpine schistose basement; 2) Marine conglomerates; 3) marine heavily bioturbated grey marls, with thin (sometimes disturbed) sandstone beds; 4) incising channel fans (channel complex); 5) very fine grained sandstone-siltstone couplets as thick sheet deposits of mainly metamorphic provenance (Unit C in Haughton 2000); 6) many thin bedded and graded sand sheets (turbidites), sporadically alternated by thick mass flow (tripartite) deposits (termed megabeds); 7) Shallow marine sand and mudstones followed by evaporites; 8) Unconformably (angular) overlying marine deltaic conglomerates and mudstones; and 9) alluvial fan conglomerates. Of these stages, the very fine grained thick sheet deposits (nr. 5) and especially the turbidites with megabeds (nr. 6) cover most of the stratigraphic interval (hundreds of meters): these are the sediments on which we focus our study.

Biostratigraphy

A previous study has shown two biostratigraphic marker-species to be present in the Tabernas basin, namely *Globorotalia conomiozea (G. conomiozea)* and *Neogloboquadrina humerosa* have been placed in a composite section (Kleverlaan, 1989b). Two megabeds have been recognized above the GMB and are interpreted to be of Messinian age since they are positioned stratigraphically above the *G. conomiozea* which defines the Tortonian/Messinian boundary at 7.24 Ma (Hilgen et al., 1995). The GMB is placed below this biostratigraphic marker and above the *Neogloboquadrina humerosa*, a species with a First Occurrence (FO) of 8.5 Ma (Berggren et al., 1985), resulting in a Late Tortonian age (between 8.5 and 7.24 Ma). The biostratigraphic samples for the study had been retrieved from an area near one of the sections used to construct the composite section southwest of Tabernas, the exact sampling location being unclear. As a result the author concludes that the age of the composite section which comprises the megabeds is roughly between 7 – 8 Ma (Kleverlaan, 1989b).

Section

The section is located southwest of Tabernas (Fig. 1), north-west of the junction between the A-92 and N-340a motorways, named after the bridge 'Puente de Los Callejones' spanning the river(bed) 'Rambla de Tabernas'. It is the same section Haughton (2000) studied to establish an initial stratigraphy and depositional history of the succession but with and upward extension of younger sediments (above Unit E, i.e. the GMB). The section is divided into three parts;

1) East section (light green, Fig. 1), located in a north-west to south-east (NW-SE) orientated slightly incised riverbed which is usually dry. In the narrow part of the riverbed, at the 0-200 m stratigraphic level, the section is excellently exposed in the steep sides of the riverbed. From 200 m onwards, the exposure is good, on the washed clean horizontal surface at the top of the riverbed (less erosional incision). West of the section, at a stratigraphic level of 263 m, the base of the GMB is exposed, but the contact to the seemingly continuous turbiditic succession in the section is unclear (see Discussion). From 263 m onwards, the section is less well exposed.

A near vertical NW-SE trending apparently dextral fault with minor horizontal (strike-slip) displacement, is located in the river-bedding, but individual beds are easily correlated on either side of the fault and displacement can be estimated to be about 25 m average (decreasing towards the south-east). The overall stratigraphy is dipping to the WNW at a 30° angle, although a total variation of 20 degrees in both strike and dip can be observed throughout the section, presumably related to different amounts of fault drag.

2) West section (dark green, Fig. 1), located west of the high NW-SE orientated ridge where exposure is good along the base of the ridge. The same dextral near vertical NW-SE trending fault (Fig. 2) as in the East section runs through the section and unfortunately the vertical displacement could not be established by correlation of (marker-)beds. Fault drag on either side of the fault suggest that displacement along the fault has a vertical component which is likely the main component. When assessing vertical displacement, it can

be calculated, using the (visual) horizontal displacement from the East section of 25 m, the dip of the stratigraphy and the almost perpendicular orientation of the fault to the strike of the stratigraphy in the East section. This vertical displacement can be calculated to be less than 20 m (tan(35°)×25 m≈18 m). The estimated amount of stratigraphy not exposed by this fault is about 10 meters, subtracting an 8m overlap of the 20 m displacement (Fig. 2). The stratigraphy in the West section is dipping steeply to the NW with an average dip angle of 50°, dipping especially steep (70°) near the major fault zone north of the section, oriented at the W-E dirt road with a steel gate. Fractures and small scale faults are increasingly present when nearing the top of the West section (towards the gate).

3) The North section (blue in Fig. 1, Fig. 3), located north-east from the West section, is exposed in a NW-SE orientated ridge with addition of a parallel ridge to the west running up to an erosional unconformity with sub-horizontal conglomeratic river deposits of Quaternary age on top (Kleverlaan, 1989a). The stratigraphy is dipping NW, with an average dip of 35°, dipping steep (50°) at the base and gradually shallowing at the top (20°), near a SW-NE orientated hinge of a syncline just north of the section (partly covered with Quaternary sub-horizontal deposits). The lower part of the section, from the base of the ridge to the end of the first ridge, has excellent exposure, in most part caused by the road cut of the old road, located west of the current A-92 motorway. This trajectory is followed up to a large curve to the right, from where the section can be continued on top of the ridge by visually tracing individual (hard) layers in the field. From the ridge onwards, to likewise correlated subsections to the west, exposure of especially mudcaps and soft alternations is decreasing.

Figure 2. Vertical low displacement fault in West section (dividing lower and upper West sections). Subtracting the 8 m overlap from the estimated 18 m displacement results in a ~10 m stratigraphic gap.

Puente de Los Callejones North section
Tabernas

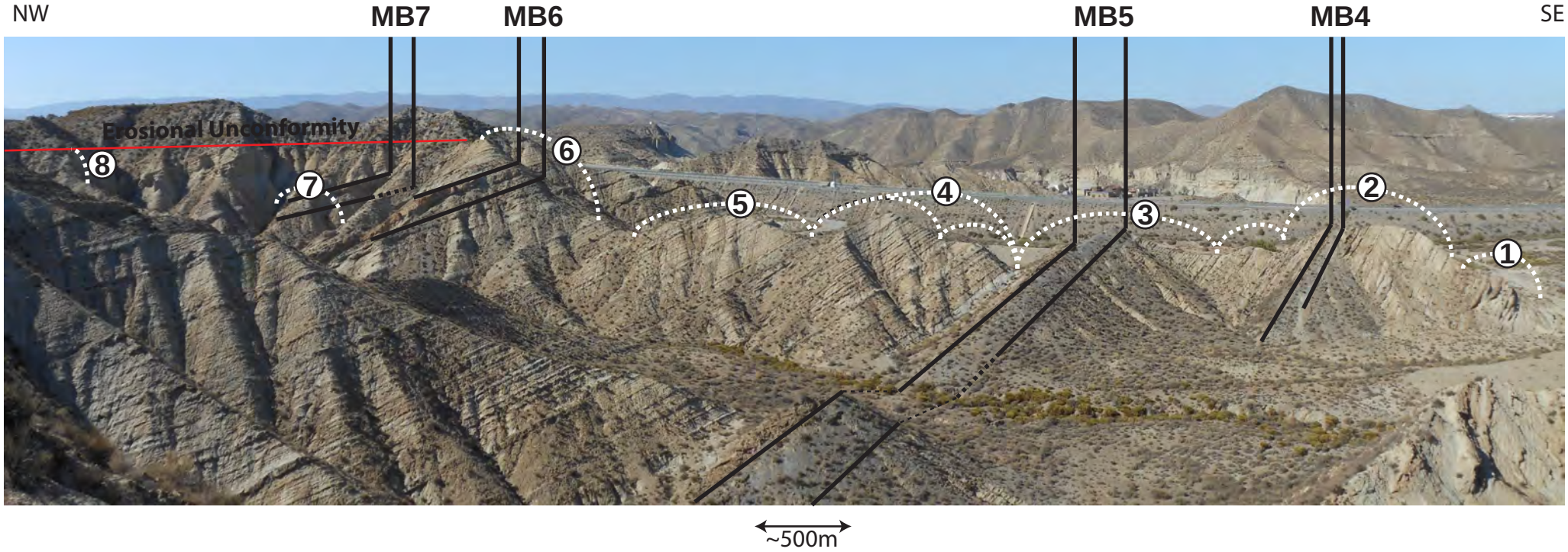

Figure 3. Overview of the North section corresponding with the stratigraphic column of figures 7 and 8. Numbers at the ridges can be used for easy correlation to the stratigraphic column and megabeds are indicated. Note that from arc nr 6 to 8 the stratigraphy was actually measured on the ridge running up to arc nr 8, not visible from this viewpoint, with the last part of the section just visible right below the erosional unconformity.

North of the major fault zone and slightly West of the North section, an additional 100 m of stratigraphy is exposed in a parallel ridge to the North Section, which was not included due to lack of time. These sediments fill up the stratigraphic gap between the West and North section.

Material and Methods

Using the section locations described above, the lithology of all sections was logged, starting furthest south-east in the East section, at the stratigraphic base, subsequently followed by the West and North sections according to stratigraphic order. Stratigraphic thickness measurements were either made with measuring tape (on thin beds) or by using an improvised Jacob's staff consisting out of 2 aluminum 1.5 m long bars with 5 cm interval scale-marks, together with a compass for getting the stratigraphic thickness consistent with the bedding orientation (bar perpendicular to bedding). All individually recognizable beds thicker than 10 cm were logged, determining grain size according to the Wentworth scale at the bottom and top of the bed to indicate their grading (common). Relief, color variation, bioclastic content, bedforms and sedimentary structures were recorded for each bed. Soft layers less than 10 cm thick usually consisting of a matching pair (couplet) of a courser grained turbiditic base and associated overlying mudcap (according to several stages of the Bouma sequence (Bouma, 1962)) were grouped into 'soft alternation' intervals. The stratigraphic thickness of the interval was then measured and the number of turbiditic couplets counted, indicating the average thickness of individual turbiditic events within a 'soft alternation' group. Logging of the stratigraphy focuses most on the stratigraphic thicknesses and different lithologies and their depositional style, creating a framework for biostratigraphy and magnetostratigraphy. Less focus is placed on sedimentary structures (ripples, flow directions, bioturbation, etc), which have already been extensively studied in the area (Kleverlaan, 1987, 1989b; Haughton, 2000, 2001).

The most important tool available for obtaining an accurate age model is the planktonic foraminiferal biostratigraphy, by identification of several marker-species which have been accurately dated in astronomically tuned continuous deep marine sediments from the Mediterranean (Hüsing et al., 2009 and references therein). For each section, large samples of at least 1 kg/sample were taken at roughly 3 m spacing intervals, with each sample being carefully selected for the presence of foraminifers by visual inspection with a hand-lens. It was experienced that especially thin alternations of turbidites contained foraminifers, since these represent relatively quiet periods in the basin history and likely comprise more time than thicker turbidites. Sometimes very thin hemipelagic layers with a maximum of only a few millimeters thickness are found between the thin turbiditic alternations where the concentration of foraminifers is moderately high. However, in general, foraminiferal yield is extremely low with less than 1% (mass) content, often their concentration is around 0.1% with the residual material being (lithic) silts and sands. In order to retrieve the foraminiferal assemblage from the samples, all samples were sieved with a standard US-120 (125 µm) brass sieve, still resulting in large sample volumes which were then processed with a high-density fluid separation method according to the method described by Semensatto and Dias-Brito (2007). The high-density fluid was prepared by dissolving Zinc-chloride (technical grade) in demineralized water, until a density of 1.71 gmL^{-1} was reached, measured with a Mettler Toledo Densito 30PX. The dried sieved product of each sample was introduced to the fluid in a standard 150 ml beaker and thoroughly mixed, after which the foraminiferal tests started floating and (lithic) silts settled on the bottom. The fluid with floating foraminifers is separated from the sediments by simple decantation and poured onto a filter (Cellulose ashless grade, 4-12 µm particle retention) placed in a Büchner funnel with an applied vacuum. The foraminifers are subsequently rinsed with demineralized water, dried and labeled after which species determination is performed. For a more detailed description of the density separation process, see appendix 2.

When assessing the planktonic foraminiferal assemblages, the taxonomic concept that is widely used in the Mediterranean was applied (Hilgen et al., 1995; Krijgsman et al., 1997; Sierro et al., 2001), with astronomical ages for bio-events recalculated to La2004 (Laskar et al., 2004) according to the ATNTS2004 (Hüsing et al., 2009). Analyses were done according to the semi-quantitative methodology of Rio et al.

(1990), comparable to the study on the Monte del Casino (Krijgsman et al., 1997), one of the Late Miocene reference sections.

In addition, all sections were sampled with an average spacing of 6 meters for magnetostratigraphy. Samples were taken with a handheld electric drill equipped with a diamond tip core drill bit and oriented in the field. Sample levels were selected on the basis of their lithology with preference for fine grained (<silt) homogeneous sediments, which generally yield a higher quality primary component of the Natural Remnant Magnetization (NRM)(Dupont-Nivet and Krijgsman, 2012).

Often these sediments were marls, mudcaps and soft alternations (fine grained parts), described as lithologies 1, 5 and 6. About half the sample levels were selected for thermal demagnetization (evenly divided over the sections); each specimen was thermally demagnetized in a magnetically shielded, laboratory-built furnace using small temperature increments of 30°C. At most sample levels a specimen was selected for alternating field demagnetization, starting with steps of 5 mT until 50 mT and continuing with 10 mT steps up until 100 mT. In both cases the NRM was measured on a 2G Enterprise horizontal cryogenic magnetometer equipped with DC SQUIDS (noise level equal or less than 3×10^{-12} Am^2). The directions of the NRM components were calculated by principle component analysis (Zijderveld, 1967; Kirschvink, 1980).

Results

Lithostratigraphy

The detailed logs of the sections are presented in Appendix 1, which include all sample locations for biostratigraphy and magnetostratigraphy. A condensed version of the stratigraphy with foraminiferal and paleomagnetic data is compiled in Figures 4, 5, 6 and 7. In total, six main lithologies were identified;

1) Structureless thick grey marls. Sometimes a vague disturbed bedding is visible. This lithology is only present in the lowest part of the section.
2) Turbiditic layers, composed of mainly lithic (phyllitic) sand and often distinctly graded (fining upwards). At the base, these layers can contain larger grains, often up to granule size and sometimes above. Occasionally fragmented shells are present in the coarser part of the layer, while in the top part, ripples or laminations can sometimes be found.
3) Mass flow deposits, consisting of a combination of deformed layers of turbiditic origin, rip up clasts (brown to grey mudstones), grey structureless silts and sometimes lithic clasts. Even though these layers can be clearly recognized from turbiditic beds by their distinct internal structure, the appearance of each mass flow deposit can be different depending on their composition.
4) The Megabeds, previously studied by Kleverlaan (1987, 1989) and Haughton (2000), are a special group of mass flows because of their vast thickness and their often large portion of coarse lithic fragments (commonly schistose cobbles/boulders). Megabeds 5, 6 and 7 do contain much lower fractions of lithic material and are therefore, except for their thickness, comparable to lithology 3 mass flows.
5) Siltstone caps (or mudcaps), consisting of mainly lithic grey to black silts, can be found right above the turbiditic layers and mass flow deposits. They are deposited in the waning of the flow caused by the slump or turbidite and consist partly of material which has been in suspension as a result of the event (equivalent of unit D and E_t of the Bouma sequence), subsequently covered by pelagic mudstone (equivalent of unit E_p of the Bouma sequence) (Bouma, 1962; Kleverlaan, 1987). Often the pelagic mudstone is thin or can not be distinguished from underlying siltstones.
6) Soft alternations, consisting of thin turbidites with their corresponding mudcaps.

The East section contains grey marls at the base, without much visible structure and only some turbiditic thin sandy beds, with an upward progressively increased fraction of turbiditic layers, up until 35 m where the first thick turbidite with corresponding mudcap (total of 1.5 m) is found. Above this level, the thick structureless marls are not present anymore and alternations of thick and thinner turbidites with their

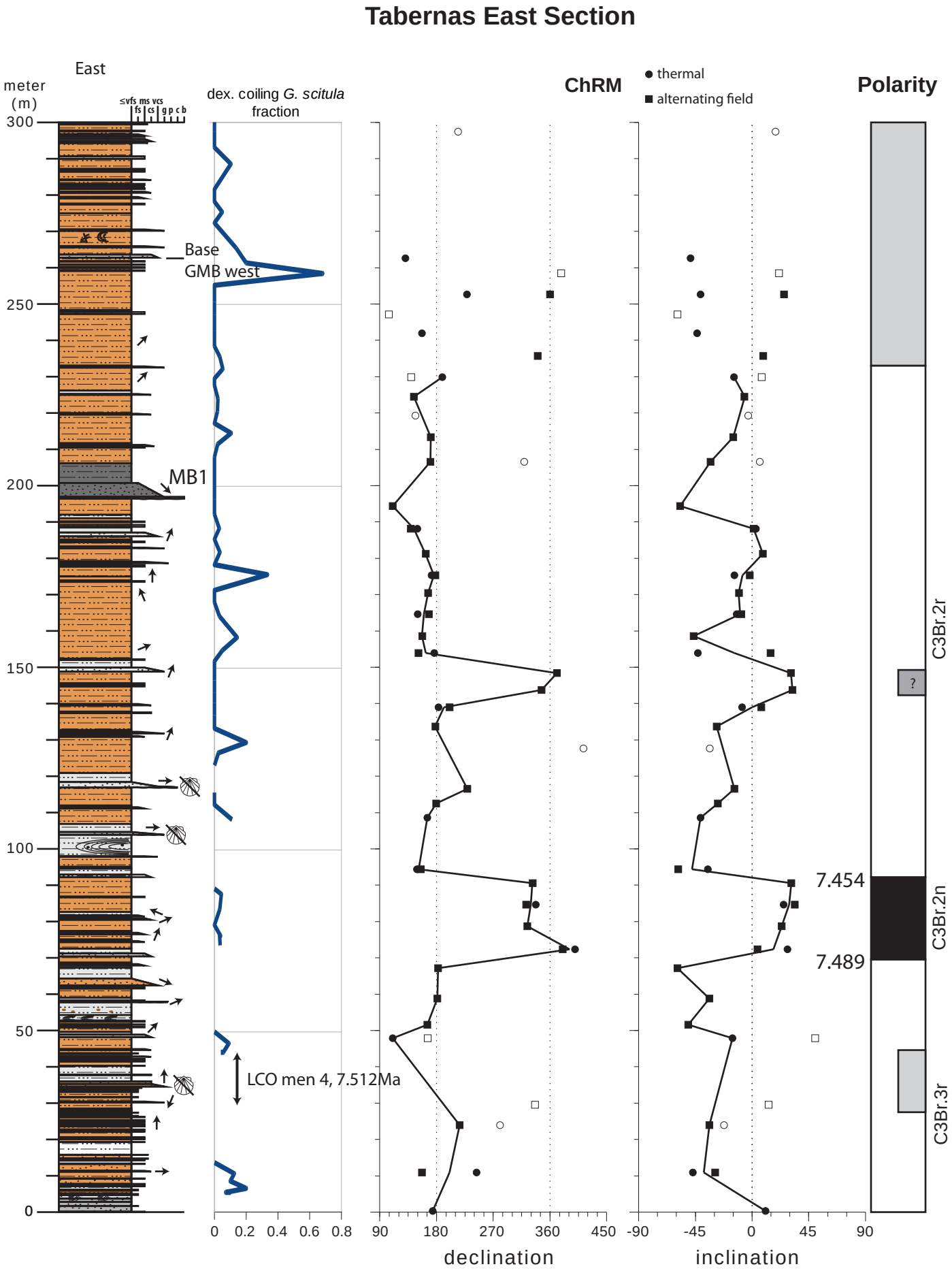

Figure 4. Stratigraphy, biostratigraphy and magnetostratigraphy of the East section.

Tabernas West Sections

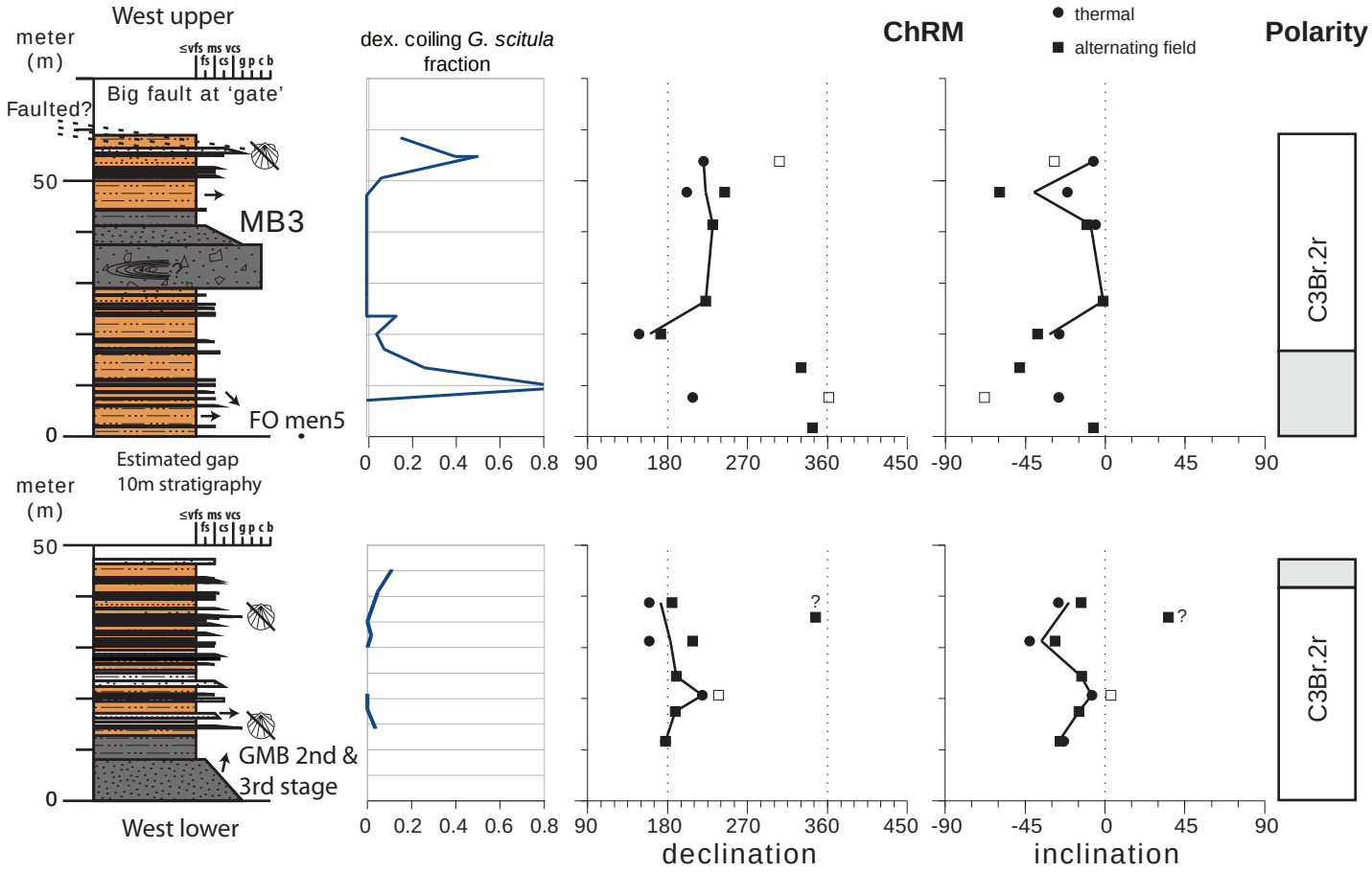

Figure 5. Stratigraphy, biostratigraphy and magnetostratigraphy of the West sections.

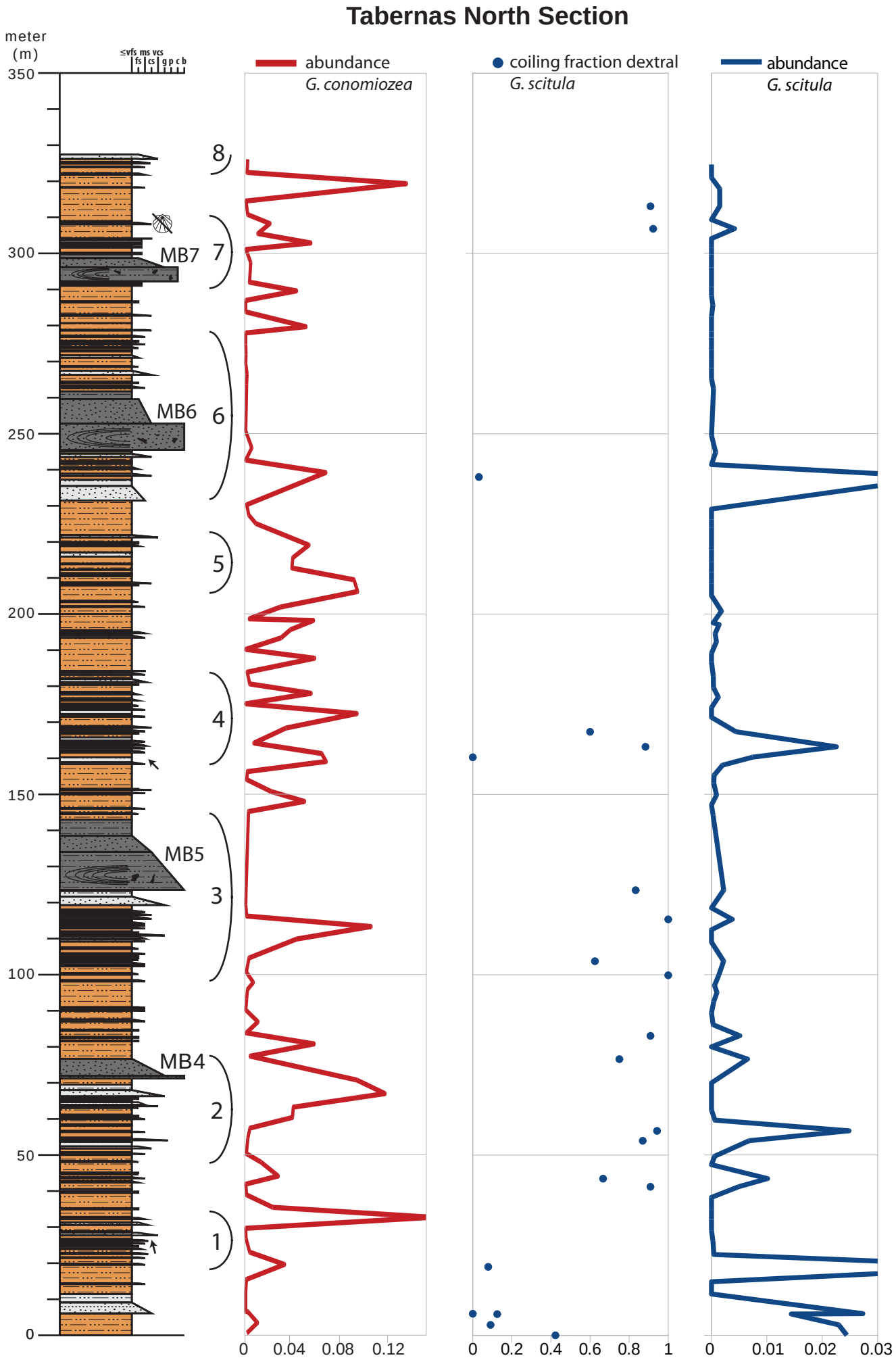

Figure 6. Stratigraphy and biostratigraphy of the North section.

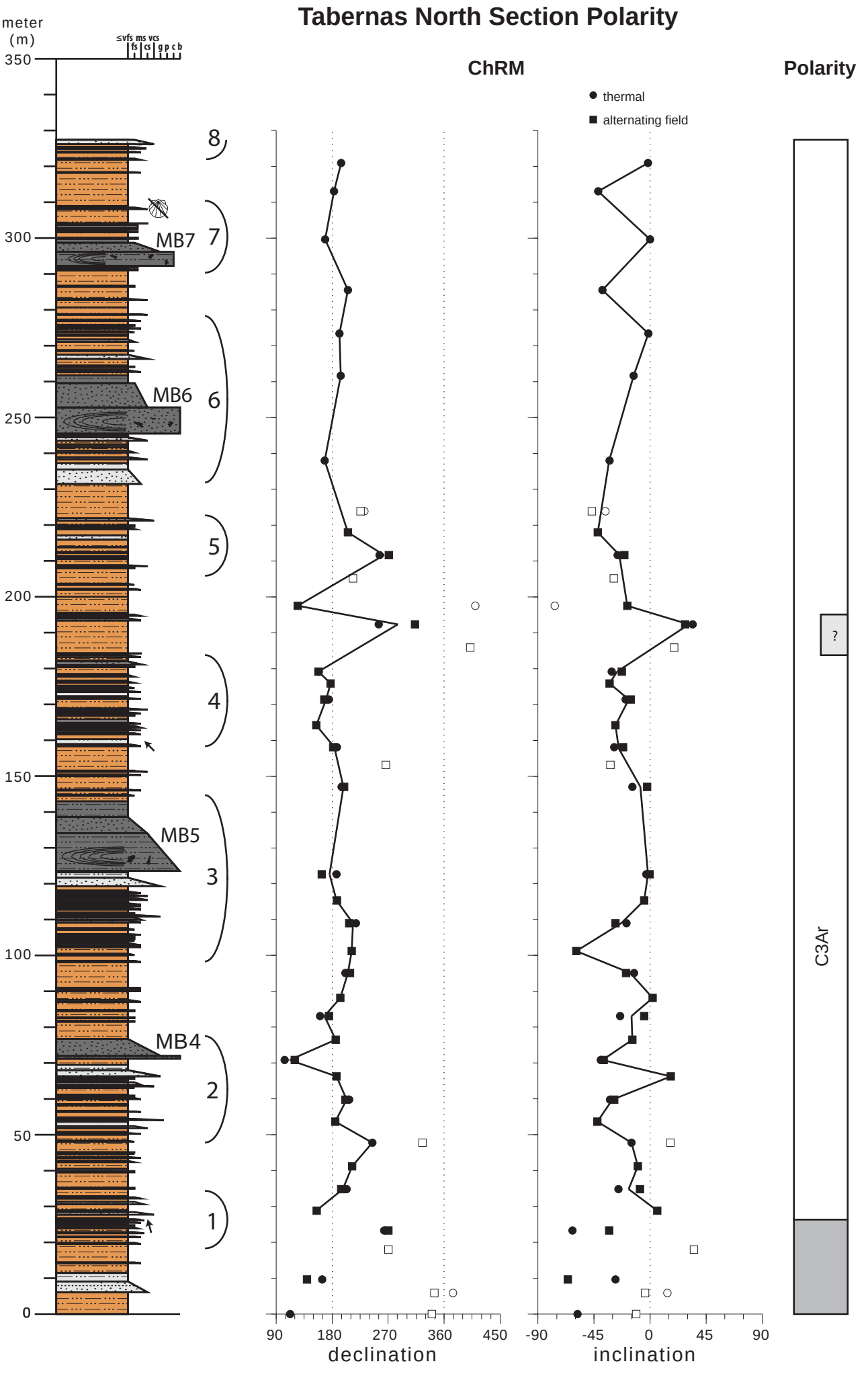

Figure 7. Stratigraphy and magnetostratigraphy of North section

mudcaps represent the main lithology, sporadically alternated by deformed layers of turbiditic origin which are interpreted to be mass flow deposits (slumps), for example at 53 m where a 2 m thick layer of deformed turbiditic strata can be found. At 196 m, the first 10 m thick Megabed (MB1) can be found, with the characteristic division as described by Kleverlaan (1987). At 263.6 m, the base of the second Megabed, also known as the GMB, is found, even though turbiditic layers seem to continue conform the regular stratigraphic succession when positioned about ten meter to the north-east. The contact between the GMB deposits and this seemingly continuous stratigraphy is unclear, however the layers at this level have some faults or internal deformation (depicted at 268 m), while exposure is less well in this part of the section. The section is logged and sampled until exposure is hindered by vegetation (by lacking erosional incision).

The West section starts on the GMB, at the contact of the lower mass flow deposits with large lithic clasts and the successive lithic sands. The thickness of the GMB in total has been calculated to be 40 m, by using GPS and the GMB orientation, 100 m south-west of the start of this section. The lower part of the section consists of the second and third stage of the GMB followed overlying turbiditic sediments and is continuous up until the near vertical fault (see section description), which introduces an estimated gap of 10 m in the stratigraphy. In the upper part of this section, after the fault, the turbiditic succession is progressively fractured and faulted towards the E-W fault zone located in the small pass between the NW-SE orientated ridges (at the steel gate). The base of Megabed 3 can be found at 29 m in the upper part of the section and comprises about 15 m of stratigraphy. The section continues until certainty of a continuous stratigraphy is lost due to complex faults at the major fault zone (at 59 m).

The North section consists of similar strata as the stratigraphic succession below the major fault zone and is continuous for 330 m. This succession contains several Megabeds at 71 (MB4), 124 (MB5), 245 (MB6) and 292 m (MB7)(position of the base), consisting of an upwards decreasing fraction of large lithic clasts and increasing fraction of deformed turbiditic layers and grey muds.

The East and West sections are correlated by visual tracing of the GMB in the field. In the upper part of the East section, at 263.6 m the base of the GMB can be traced to the west, where the West section starts on top of the mass flow deposits and the thickness of the megabed is well constrained to 40 m in total (measured by GPS). The Lower and Upper West section can be correlated quite accurately by estimation of the stratigraphic gap, of about 10 m. This brings the total stratigraphy at a total of 730 m, 400 m in the East-West section and 330 m in the North section, missing an additional 100m of stratigraphy at the base of the North section (see section description).

Biostratigraphy

Most samples yield an adequate number of foraminifers (>500 foraminifers counted) with moderate to good preservation quality. The lowest yields are found in samples from the first 100 m of the East section (Appendix 3 for detailed overview). Several marker-species and distinctive bio-events (Table 1) are found in the sections, namely the Last Common Occurrence (LCO) of *G. menardii 4*, the First Occurrence (FO) of *G. menardii 5* and the marker-species *G. conomiozea* (*miotumida*)(Fig. 4, 5 and 6). The relative abundance of *G. scitula* and *G. conomiozea* (only in North section) is established complemented by the coiling direction of *G. scitula*. Only samples with 5 or more specimen of *G. scitula* are included in the coiling direction record to enhance its reliability.

Magnetostratigraphy

The results show that the Last Occurrence (LO) of *G. menardii 4* is located between 29.55 and 44.40 m in the East section, which could not be established in more detail because the samples between those positions have a low foraminiferal yield. The FO of *G. menardii 5* is located in sample 05-09, positioned directly at the base of the upper part of the West section, above the small displacement fault. Throughout the North section, *G. conomiozea* is found with the exception of some barren intervals at the top of the section.

The results from the principle component analysis show that for 90% of the samples a ChRM direction can be obtained for both thermal (TH) and alternating field (AF) demagnetization after tectonic correction (tc). Diagrams generally show two components, the first one (A) is present in the first few (temperature or

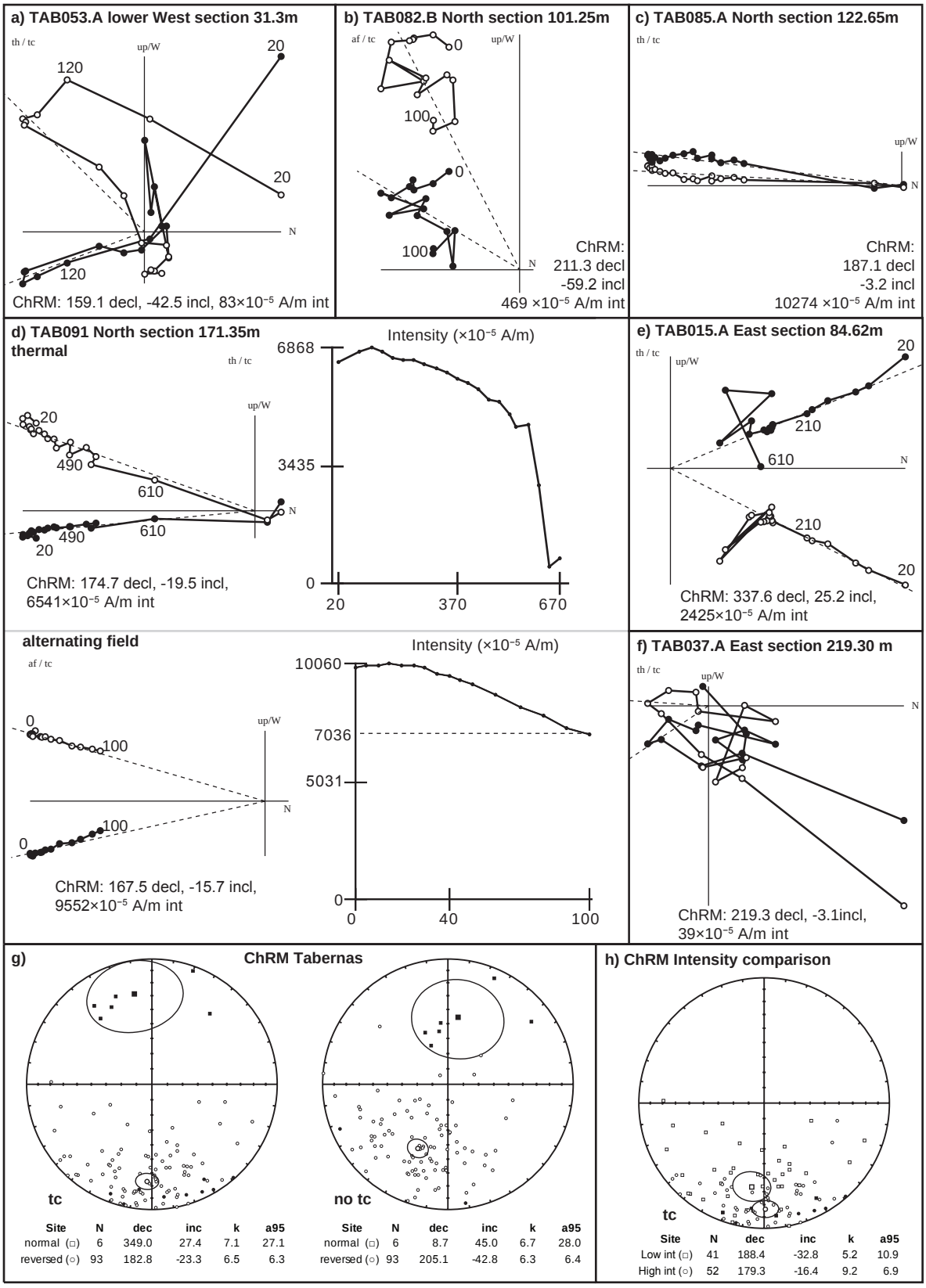

Site	N	dec	inc	k	a95
normal (□)	6	349.0	27.4	7.1	27.1
reversed (○)	93	182.8	-23.3	6.5	6.3

Site	N	dec	inc	k	a95
normal (□)	6	8.7	45.0	6.7	28.0
reversed (○)	93	205.1	-42.8	6.3	6.4

Site	N	dec	inc	k	a95
Low int (□)	41	188.4	-32.8	5.2	10.9
High int (○)	52	179.3	-16.4	9.2	6.9

Figure 8. Paleomagnetic data Tabernas sections. tc=tectonic correction, th=thermal demagnetization, af=alternating field demagnetization. a+b) Samples with low intensity component. c+d) Samples with high intensity normal polarity. e) Sample with normal polartiy (high intensity). f) Sample with unreliable component, reverse polarity. g) Plot of reliable ChRM directions (black dots/squares in magnetostratigraphic columns) which have an interpreted polarity (thus points used to construct the black line in the magnetostratigraphic columns). Shows ~25° declination offset for 'no tc' ChRM directions. Inclination is low, especially for tc samples. h) Comparison of reverse polarity ChRM directions by division in a high intensity (>1000×10⁻⁵ A/m) and low intensity (<1000×10⁻⁵ A/m) group. Shows inclination shallowing by high intensity magetic carrier.

alternating field) steps, mainly in the range of 20-120°C or 0-10 mT. This component is the Viscous Remanent Magnetization (VRM). The second component (B), is interpreted as the NRM and is found in many steps after component A, often from 120-670°C or 15-100 mT and can can be subdivided into two groups; 1) Low intensity group (Fig. 8a and b) with directions generally consisting of demagnetization steps up to 400°C or 80mT; 2) High intensity group (Fig. 8 c-e) with directions based on a larger number of demagnetization steps up to 670°C or 100mT. For some samples (Fig. 8f) a reliable ChRM direction can not be obtained, caused by low intensity and scatter.

The high intensity of B2 samples is stable up to ~600°C, after which the intensity decreases rapidly in a narrow temperature range (Fig. 8d). When applying alternating field demagnetization, these samples do not show significant demagnetization up to 100 mT (the maximum), with a minor decrease of intensity to about 70%. This magnetic mineral behavior is most consistent with hematite. The low intensity B1 samples show a variety of demagnetization characteristics, Isothermal Remanent Magnetization (IRM) acquisition (and fitting) is needed to determine their magnetic mineral(s).

Overall, the Characteristic Remnant Magnetization (ChRM) directions show mainly reverse polarity (Fig. 8 a-d and f), except for the interval from 70-90 m in the East section which displays a clear normal polarity (Fig. 8e).

Plotting all ChRM directions (● = reliable, ○ = unreliable) at their respective stratigraphic sample levels (Fig. 4, 5 and 7), reveals a consistent polarity pattern, although the variation of the obtained ChRM directions is high. At several levels polarity could not straightforwardly be interpreted and are visualized by grey polarity intervals. The correlation of the polarity intervals to the ATNTS2004 (Lourens et al., 2004) is presented below (Age model).

All reliable ChRM directions which could be synthesized into a polarity interpretation (line connected black dots/squares on Fig. 4, 5 and 7) are plotted on a Stereonet (Fig. 8g), both with and without tectonic correction. Due to the low number of normal polarity samples it is not possible to statistically prove that normal and reverse polarity groups are antipodal but the location of the mean averages and their a95 confidence circles tentatively show that they share a common true mean direction. Furthermore, the reverse sample group shows that the mean declination direction is well constrained at 182.8° (a95 = 6.3°), while the same ChRM directions without correction show a declination of 205.1° (a95 = 6.4°). Comparing these declinations clearly shows that the obtained ChRM directions are pre-tilting since these yield the ~180° declination expected for the age and location of the section (Krijgsman and Garces, 2004), while tectonically uncorrected samples show a 25° rotation. When assessing the average inclination of -18 to -30° (TC and considering a95 probability) it is evident that this angle is very shallow compared to the expected inclination of ~-50° at this (paleo-)latitude. It is common in fine grained marine sediments (clays) to experience inclination shallowing, induced by compaction of the sediments after deposition, but the magnitude of shallowing usually is around 5-15 degrees (Anson and Kodama, 1987; Deamer and Kodama, 1990), depending on the amount of compaction and the degree to which the magnetic carrier particles are able to rotate during compaction (in itself depending on many factors).

All the reliable reverse ChRM directions (from Fig. 8g) are divided into a high (>1000 $\times 10^{-5}$ A/m) and low (<1000 $\times 10^{-5}$ A/m) intensity group, representing their different carriers, after which the average inclination of the groups can be compared (Fig. 8h). The results show that the high intensity group has a significantly shallower inclination of ~-16° compared to the ~-32° of the low intensity group. Hematite is known for substantial inclination shallowing (in red beds) (Iosifidi et al., 2010) and this can be causing the considerable inclination shallowing of the high intensity group. Comparison of the low intensity group inclination with an average of ~-32° inclination to the adjacent Sorbas basin where the Abad marls report an average of ~-36° inclination (Krijgsman and Garces, 2004), shows that inclination shallowing is equally significant in both basins. The high intensity samples visually do not seem to contain large amounts of red pigmentary (red bed like) hematite, so it is expected that all hematite is specular (black). The low amounts of expected hematite and the observed high intensities indicate that the ChRM might be carried by a titanium bearing ilmenite-hematite inter-growth complex which acts as a lamellar magnetic material, while still retaining similar properties as single-domain hematite (Robinson et al., 2002).

Marker events

Planktonic foraminifer	Event	Age (Ma)	Stratigraphic position
Globorotalia nicolae	FO	6.835 ± 0.007	
Globorotalia scitula dextral	Reduction	7.007[2]	North section, ~170 m
Globorotalia conomiozea	FO	7.243 ± 0.003	North section, base
Globorotalia menardii 5	LO	7.260[2]	
Globorotalia menardii 4	Influx	7.289[1]	
Globorotalia menardii 5	FO	7.372 ± 0.002	West upper section, 0.80 m
Catapsydrax parvulus	LO	7.440-7.446[1]	
Globorotalia menardii 4	LCO	7.515 ±0.002	East section, 29.55-44.40 m
Magnetic polarity changes	**Old (Ma)**	**Young (Ma)**	**Stratigraphic position**
C3Ar	7.140	6.733	North section
C3Bn	7.212	7.140	
C3Br.1r	7.251	7.212	
C3Br.1n	7.285	7.251	
C3Br.2r	7.454	7.285	Old at East 90.52 – 94.42 m
C3Br.2n	7.489	7.454	Old at East 67.12 – 72.35 m, Young at East 90.52 – 94.42 m
C3Br.3r	7.528	7.489	Young at East 67.12 – 72.35 m
C4n.1n	7.642	7.528	

Table 1. Ages of bio-events, magnetic polarity changes and their respective stratigraphic positions (when applicable), biostratigraphic ages from Hüsing et al. (2009). [1] Ages from Krijgsman et al. (1997). [2] Ages from Sierro et al. (2001). Magnetic polarity ages from ATNTS2004 (Lourens et al., 2004).

Age model

Section and sedimentation rates

The clear biostratigraphic events and their location in the sections demonstrates that reworking of sediments is not of significant influence and the planktonic foraminifers found in the fine grained sampled lithologies are seemingly trapped in the sediment as a regular flux from the water column to the seafloor (hence their low concentration). Both the East-West composite and North section can be independently correlated to the ATNTS2004 (Lourens et al., 2004) by biostratigraphic events and polarity changes (Fig. 9). Additionally, a comparison to the Monte del Casino section (Krijgsman et al., 1997) is made, since this section has the most accurately described biostratigraphy of the Mediterranean sections spanning this interval, including relative abundances of *G. conomiozea* and *G. scitula*, with additional coiling direction of *G. scitula*.

Both the LCO of *G. menardii 4* (7.515 Ma) and FO of *G. menardii 5* (7.372 Ma) can be located in the East-West composite with an uncertainty of 10-15 m. At the base of the section, sinistral *G. scitula* can be found together with *G. menardii 4*, implying an age younger than the reappearance the *G. menardii 4,* which has been dated at 7.54 Ma in the Monte del Casino section, but older than its LCO at 7.515 Ma. In the top part of the East-West section, *G. menardii 5* is found, implying an age younger than its FO dated at 7.372 Ma, while the influx of *G. menardii* 4, dated at 7.289 Ma, is not reached. Based on these biostratigraphic constraints, the polarity pattern of the East-West composite could be straightforwardly correlated to the ATNTS2004, yielding two additional calibration points; 1) base of chron C3Br.2n at 7.489 Ma; and 2) top of chron C3Br.2n at 7.454 Ma.

These combined age constraints yield a minimum and maximum duration for the East-West composite section of 143 kyr (7.515-7.372 Ma) and 230 kyr (7.54-7.31 Ma), respectively. Sedimentation rates can be

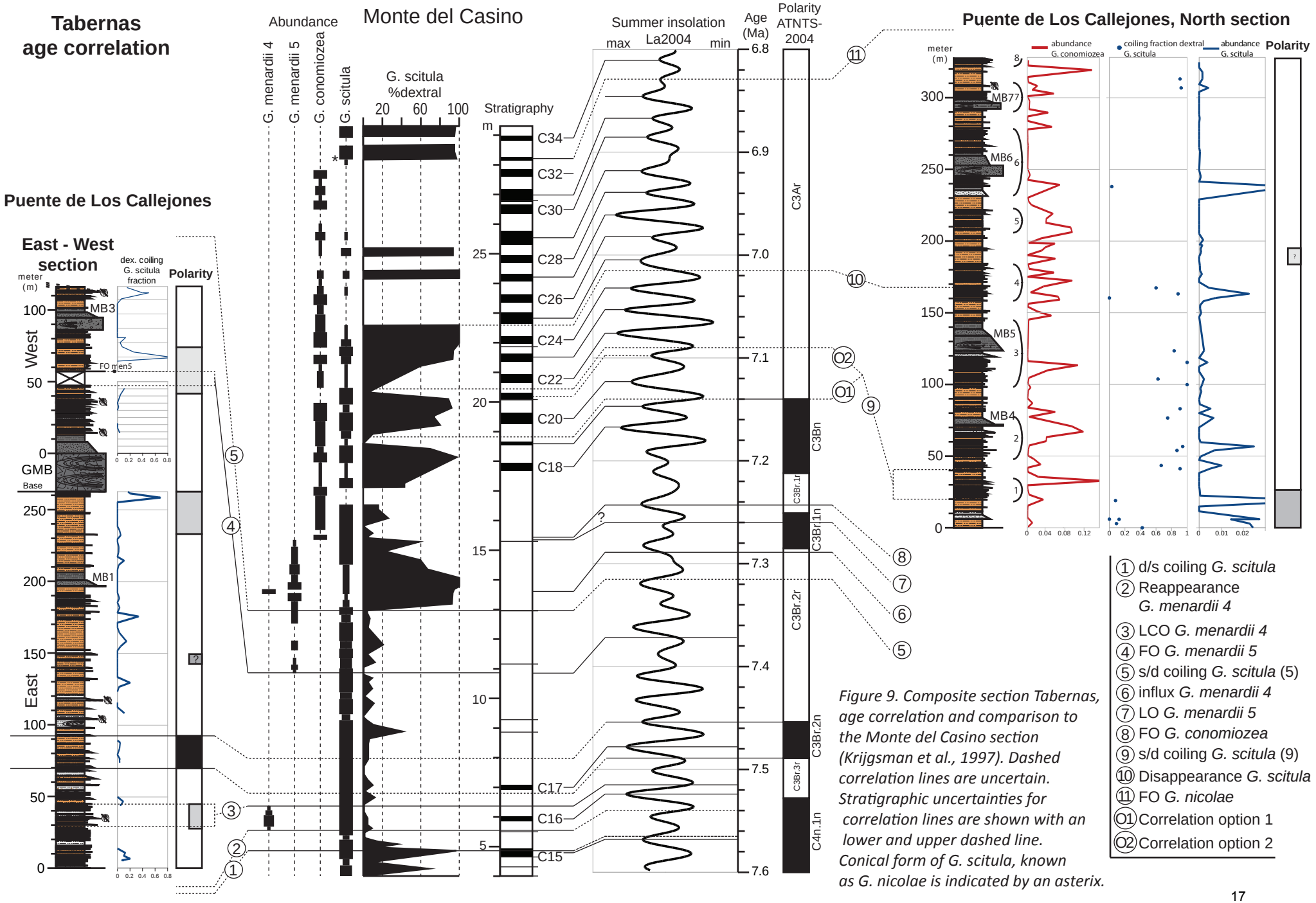

Figure 9. Composite section Tabernas, age correlation and comparison to the Monte del Casino section (Krijgsman et al., 1997). Dashed correlation lines are uncertain. Stratigraphic uncertainties for correlation lines are shown with an lower and upper dashed line. Conical form of G. scitula, known as G. nicolae is indicated by an asterix.

Overview of age, stratigraphic thickness and sedimentation rate

East-West composite	Age (Ma) Min	Max	Average	+/-	Stratigraphy (m) Min	Max	Average	+/-	Sedimentation rate (m/kyr) Min	Max	Average	+/-
LCO *G. menardii 4*	7.513	7.517	7.515	0.002	29.55	44.40	36.98	7.43				
Base C3Br.2n	7.489	7.489	7.489	0	67.12	72.35	69.74	2.62				
Δ	**0.024**	**0.028**	**0.026**	**0.002**	**22.72**	**42.80**	**32.76**	**10.04**	**0.81**	**1.78**	**1.30**	**0.49**
Base C3Br.2n	7.489	7.489	7.489	0	67.12	72.35	69.74	2.62				
Top C3Br.2n	7.454	7.454	7.454	0	90.52	94.42	92.47	1.95				
Δ	**0.035**	**0.035**	**0.035**	**0**	**18.17**	**27.30**	**22.74**	**4.57**	**0.52**	**0.78**	**0.65**	**0.13**
Top C3Br.2n	7.454	7.454	7.454	0	90.52	94.42	92.47	1.95				
FO *G. menardii 5*	7.370	7.374	7.372	0.002	338.10	348.10	343.10	5.00				
Δ	**0.080**	**0.084**	**0.082**	**0.002**	**243.68**	**257.58**	**250.63**	**6.95**	**2.90**	**3.22**	**3.06**	**0.16**
Δ without MB1 and the GMB					**193.98**	**207.88**	**200.93**	**6.95**	**2.31**	**2.60**	**2.45**	**0.14**
LCO *G. menardii 4*	7.513	7.517	7.515	0.002	29.55	44.40	36.98	7.43				
FO *G. menardii 5*	7.370	7.374	7.372	0.002	338.10	348.10	343.10	5.00				
Δ	**0.139**	**0.147**	**0.143**	**0.004**	**293.70**	**318.55**	**306.13**	**12.43**	**2.00**	**2.29**	**2.14**	**0.15**
Δ without MB1 and the GMB					**244.00**	**268.85**	**256.43**	**12.43**	**1.66**	**1.93**	**1.80**	**0.14**
North section	**Age (Ma)** Min	Max	Average	+/-	**Stratigraphy (m)** Min	Max	Average	+/-	**Sedimentation Rate (m/kyr)** Min	Max	Average	+/-
s/d coiling change *G. scitula* (9)	7.09	7.14	7.115	0.025	19.00	41.20	30.10	11.10				
Disappearance *G. scitula*	7.01	7.02	7.015	0.005	163.20	167.35	165.28	2.08				
Δ	**0.07**	**0.13**	**0.100**	**0.030**	**122.00**	**148.35**	**135.18**	**13.18**	**0.94**	**2.12**	**1.53**	**0.59**
Δ without MB4 and MB5					**97.05**	**123.40**	**110.23**	**13.18**	**0.75**	**1.76**	**1.25**	**0.51**
Δ w/o MB4 and MB5 + best est.	**0.07**	**0.08**	**0.075**	**0.005**					**1.21**	**1.76**	**1.49**	**0.27**

Table 2a. Calculated sedimentation rates for several parts of the Tabernas sections using calibration points provided by biostratigraphic and magnetostratigraphic markers (see Fig. 9). Every set is composed of one younger (first) and older (second) event, with corresponding minimum and maximum ages and stratigraphic levels. They are cross-correlated to obtain the minimum and maximum Δ values, followed by linear interpolation of the sedimentation rate. For intervals with Megabeds, sedimentation rates are also calculated excluding their thickness. Minimum age of s/d coiling change of G. scitula is used for best estimate calculations (also in Table 2b).

Age sections

East-West composite	Age marker (Ma)	Offset to marker (m)	Calculated age (Ma)
Base (LCO *G. menardii 4*)	7.515±0.002	29.55-44.40	7.537±0.006
Top (FO *G. menardii 5*)	7.372±0.002	58.92-68.92	7.345±0.007
		Δ	0.192±0.013
North section			
Base (s/d coiling change G. scitula)	7.115±0.025	19.00-41.20	7.126±0.025
Base best estimate	7.09	19.00-41.20	7.112±0.012
Top (Disappearance G. scitula)(9)	7.015±0.005	136.25-140.40	6.882±0.060
Top best estimate	7.09	136.25-140.40	6.918±0.024
		Δ	0.243±0.085
		best estimate Δ	0.194±0.036

Table 2b. Using the sedimentation rates when excluding the megabeds and the offset from the base or top of the section to the age marker (also excluding megabed-thickness), the age and duration of both (composite) sections is calculated using linear extrapolation. Best estimate age of the base of the North section is performed with best estimate sedimentation rate (Table 2a) based on Option 2 correlation.

calculated for the intervals by linear interpolation between the calibration points (Table 2a), while thicknesses of the megabeds can be excluded to obtain a more realistic background sedimentation rate. Extrapolation of sedimentation rates using the positions of the LCO of *G. menardii 4* and FO of *G. menardii 5* while excluding the stratigraphic thicknesses of MB1 and the GMB yields an age of 7.537 ± 0.006 to 7.345 ± 0.007 Ma, and hence a duration of 192 ± 13 kyr (Table 2b) for the East-West composite section.

The North section contains a smaller number of accurate biostratigraphic events and no certain polarity changes, with only the disappearance of *G. scitula* providing a fairly accurate age of 7.01-7.02 Ma based on correlation to the Monte del Casino section (the event itself not being includied in the ATNTS2004). Since *G. conomiozea* is present throughout the section, it is certain that the North section is entirely of Messinian age. The coiling direction of *G. scitula* can not be unambiguously correlated to the Monte del Casino section, because the s/d coiling change of *G. scitula* (nr. 9 in Fig. 9) in the North section, generates two possible correlation options. Option 1 (O1 in Fig. 9) correlates the coiling change to the s/d coiling change of *G. scitula* in the Monte del Casino section dated at 7.14 Ma, coinciding with the reversal from C3Bn to C3Ar. This correlation requires normal polarities of subchron C3Bn to be recorded in the lowest part of the North section but this is not conclusive from the magnetostratigraphic data. The second option (O2 in Fig. 9) correlates the coiling change to the s/d coiling change of *G. scitula* with an estimated age of 7.09 Ma and implies a reverse polarity for the total North section. The reverse polarity of the mayor part of the North section does certainly correspond with the C3Ar subchron. At the top of the North section, dextrally coiled *G. scitula* is very scarce, this corresponds to the barren interval in the Monte del Casino section. No conical dextrally coiled *G. scitula*, also known as *G. nicolae,* is found there which implies that the top of the section must be older than 6.828 Ma (6.835 ± 0.007 Ma). Using the disappearance of *G. scitula* and both correlation options for the s/d coiling change of *G. scitula*, sedimentation rates (Table 2a) and the age of the section (Table 2b) can be calculated by following the same procedure as applied to the East-West composite section (above). This yields an age from 7.126 ± 0.025 to 6.882 ± 0.060 Ma, with a duration of 243 ± 85 kyr.

The age for the base of the North section can best be estimated using correlation Option 2 (Fig. 9) as it results in higher sedimentation rates of 1.83 ± 0.30 m/kyr for this interval then Option 1 with rates of 0.94-1.24 m/kyr. These higher rates are expected because similar high sedimentation rates are found in the top part of the East-West composite section (3.06 ± 0.16 m/kyr) and because two megabeds (MB4 and MB5) are found in the North section located between the calibration points with a combined thickness of 25m. Additionally the sedimentation rates would fit better with the observed rare influxes of *G. scitula* in the upper part of the North Section which would (in turn) better match the influxes around sapropel C28 in the Monte del Casino section. When assuming that correlation option 2 is correct, sedimentation rates and section age can be recalculated, as shown in the tables. This best estimate solution yields an age of 7.112 ± 0.012 to 6.18 ± 0.024 Ma, with a corresponding duration of 149 ± 36 kyr for the North section.

The sedimentation rates in the East-West composite section show large variations (Table 2a), with low sedimentation rates in the lower part of the section at 1.30 ± 0.49 and 0.65 ± 0.13 m/kyr and high rates in the top part at 3.06 ± 0.16 m/kyr.

Stratigraphic gap

The biostratigraphic events s/d coiling change *G. scitula* (nr. 5 in Fig. 9)(age not tuned), influx of *G. menardii 4* (7.289 Ma), LO *G. menardii 5* (7.260 Ma) and FO *G. conomiozea* (7.246 Ma) are not recorded in the sections and must be located in the missing interval between the East-West and North sections, including a potential tectonic controlled hiatus associated with the fault found on top of the East-West composite section. Because the stratigraphic gap corresponds to the FO of *G. conomiozea,* the Tortonian-Messinian (T/M) boundary is also located between the East-West composite and North section. Time not covered by stratigraphy is less than 253 kyr since the FO of *G. menardii 5* (7.372 ± 0.002 Ma) is found below the fault while the youngest correlation option of the s/d coiling change of *G. scitula* (at 7.115 ± 0.025 Ma) is located above the fault. The minimum amount of time not covered by stratigraphy is 98kyr, since the s/d coiling change of *G. scitula* (5) at 7.015 ± 0.005 Ma is not observed in the East-West composite section, while the onset of C3Br.1n (7.212 Ma) is certainly not located in the North section even if correlation option 1 is favored (coinciding with the end of chron C3Br.1n). Using the calculated age for the top of the East-West

composite section and the best estimate age for the base of the North section would result in a best estimate of 233 ± 18 kyr for the amount of time missing in the stratigraphic gap. When assessing the thickness of missing stratigraphy, this is highly dependent on the sedimentation rates. However, a sedimentation rate of ~2 m/kyr can be anticipated in view of sedimentation rates above and below, resulting in ~470m stratigraphy that is missing. The 100m section placed stratigraphically below the North section (see section description) can be subtracted from this estimate to estimate the missing stratigraphy caused by the tectonically controlled hiatus at the fault-zone (~400m of missing stratigraphy). In view of the observed stratigraphic spacing of the megabeds, it is possible that more were deposited during the time spanning this gap (and are therefore missing).

Age of the megabeds

The megabeds in the East-West section (MB1, GMB, MB3) are all confirmed to be of Late Tortonian age by the biostratigraphic results, whereas megabeds 4, 5, 6 and 7 are of Early Messinian age. The age of MB1 and the GMB must be between 7.454 and 7.372 Ma, based on their relative position to the onset of subchron C3Br.2r and the FO of *G. menardii 5*. MB3 is slightly younger than 7.372 Ma, located about 35 m above the FO of *G. menardii 5*. The in the North section located Megabed 4 and 5 are more inaccurately dated between 7.14 and 7.01 Ma, constrained by the s/d coiling change of *G. scitula* and Disappearance of *G. scitula*, whereas the newly discovered MB6 and MB7 are between 7.02 and 6.828 Ma of age (Disappearance *G. scitula* and FO *G. nicolae*).

Using the linearly interpolated sedimentation rates corrected for megabed thicknesses (Table 2a), the age of each megabed is calculated from their closest calibration point (Table 3). The megabeds in the East-West section are dated most accurately using this method, while MB4, MB6 and MB7 have ages with higher uncertainties, except when applying the best estimate sedimentation rates by assuming Option 2 correlation (Fig. 9). Our best estimates interpolation for the ages of the megabeds yields: MB1) 7.411 ± 0.003; GMB) 7.375 ± 0.018; MB3) 7.358 ± 0.005; MB4) 7.060 ± 0.013; MB5) 7.031 ± 0.009; MB6) 6.963 ± 0.016; MB7) 6.930 ± 0.022 Ma (Table 3).

Age of the Megabeds

	Age marker (Ma)	Offset with marker (m)	Calculated age (Ma)
MB1	Top C3Br.2n		
Max	7.454	106.38	7.415
Min	7.454	102.48	7.408
Average			**7.411±0.003**
GMB	FO *G. menardii 5*		
Max	7.374	44.5	7.393
Min	7.370	34.5	7.357
Average			**7.375±0.018**
MB3	FO *G. menardii 5*		
Max	7.374	38.97	7.363
Min	7.370	28.97	7.353
Average			**7.358±0.005**
MB4	s/d coiling *G. scitula*		
Max	7.14	52.2	7.123
Min	7.09	30.0	7.020
Average			**7.072±0.051**
Avg. best est.			**7.060±0.013**
MB5	Disappearance *G. scitula*		
Max	7.02	24.35	7.053
Min	7.01	20.2	7.021
Average			**7.037±0.016**
Avg. best est.			**7.031±0.009**
MB6	Disappearance *G. scitula*		
Max	7.02	76.8	6.979
Min	7.01	72.65	6.907
Average			**6.943±0.036**
Avg. best est.			**6.963±0.016**
MB7	Disappearance *G. scitula*		
Max	7.02	123.55	6.952
Min	7.01	119.4	6.845
Average			**6.898±0.054**
Avg. best est.			**6.930±0.022**

Table 3. Calculated ages for the megabeds. Calculations performed with the sedimentation rates of the interval where the megabed is positioned (Table 2a) using the closest calibration point while excluding the megabed thickness from both sedimentation rates and offset.

Comparison

A straightforward comparison of the Puente de Los Callejones section with the lithological units A-E of Haughton (2000) in the stratigraphic column of the Tabernas basin can be made (Fig. 10). Our Puente de Los Callejones section does not comprise the lower interval described by Haughton (Unit A, B and almost all of C), but does extend the succession with addition of younger sediments. Unit C, described as

Correlation to stratigraphic Units of Haughton (2000)

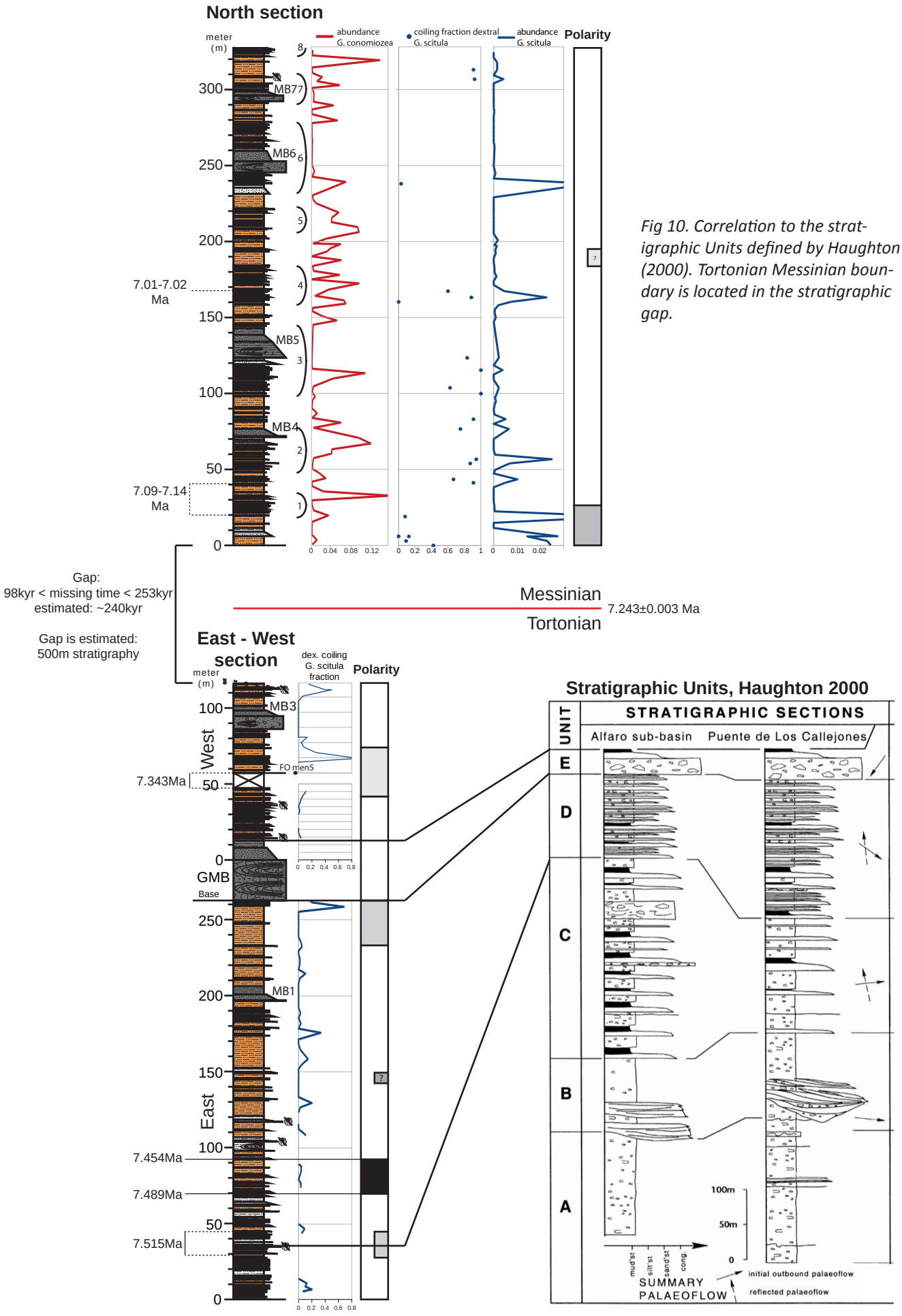

Fig 10. Correlation to the stratigraphic Units defined by Haughton (2000). Tortonian Messinian boundary is located in the stratigraphic gap.

generally thick intervals of bioturbated sandy marls intercalated with sheet-like fine grained sandstone-mudstone couplets, corresponds to the lowest part of the East section. Sandstone layers (turbidites) get increasingly more important upwards, up to 35.30 m where a thick ~1.5 m turbidite is found, followed by an increasing number of turbiditic intercalations (and less marls) described by Haughton as Unit D. The thick turbidite has a high relief (compared to the marls), a coarse granule base and contains quartz, clay rip-up clasts and shell fragments. We propose this turbidite to be the boundary between Unit C and D, and thus for correlation to the stratigraphic column of Haughton. Using this boundary, the thickness of Unit D is 228 m (263.6-35.3 m) in this section, which is in good agreement with the 200m estimated by Haughton (2000). Note that the LO of *G. menardii 4* almost coincides with the Unit C/D boundary, giving it an age of ~7.515 Ma in this section. Unit E is defined as the GMB, which can be used as a basin wide markerbed and is the uppermost stratigraphic unit in the column of Haughton. In this study, stratigraphy continues with lithologies resembling the description of Unit D, while introducing another 5 megabeds above the GMB with upwards decreasing amounts of large (boulder size) lithic fragments. Possibly this extended stratigraphy could be defined as a separate lithological unit (Unit F), since gradually the system becomes more sandy (quartz) and the supply of sediments gets more uniform (in grainsize and mineralogy). Further assessment of the sedimentological differences between the Messinian and Tortonian sediments has been out of the scope of this study.

The most reliable average sedimentation rate of the East-West composite section of 2.14 ± 0.15 m/kyr clearly shows that during the Late Tortonian the Tabernas basin was filled by sediments one order of magnitude faster than the adjacent Sorbas basin where the Messinian Abad marl was deposited at a rate of ~0.1 m/kyr (Krijgsman et al., 2001). The Monte del Casino section, with an open marine setting, had sedimentation rates two orders of magnitude lower at ~0.03 m/kyr average (Krijgsman et al., 1997).

Discussion

Origin of megabeds

Megabeds 6 and 7 in the North section have never been mapped or described and can therefore be considered to be newly discovered. Possibly they have not been identified as megabeds before because of their different appearance as they do not contain large volumes of coarse lithic fragments (schistose boulders in their first stage). However, it is evident that these thick layers represent massflow deposits, consisting of mainly deformed sedimentary material interpreted as slumped older turbiditic layers. We suggest that these younger Messinian mass flows share a common trigger with the Tortonian lithic mass flows (such as MB1, GMB, MB3), while their source material and/or their source area varies.

When observing the megabeds more closely, all seem to coincide with increased thicknesses and frequencies of the turbidites. This is especially clear in the North section which has most megabeds exposed in a continuous ridge with clear difference in the erosional profile (Fig. 3), with megabeds located in more pronounced turbiditic sequences at the more erosion resistant topographically higher parts of the ridges (marked by arches). It has been suggested that sediment overburden is not likely to have triggered the megabeds and that seismic activity is causing failure of its source material (Kleverlaan, 1987). However, it can be questioned whether alternative scenario's are also realistic. We think that several arguments re-validate this possibility. The megabeds; 1) share a sheetlike deposition style; 2) are all single event mass-flows; 3) are more common in the stratigraphic record then previously thought; 4) the system supplying mass-flow material might have been active for a long time; 5) seem to coincide with periods of increased thickness (relief) and frequency of turbidites (in the North section). Ultimately, the overburden or sediment availability might be caused by climate cyclicity (precipitation and run-off) as has been observed by (Postma et al., 1993) for turbidites on Gavdos, Greece.

The GMB does however stand out for its vast volume, lateral distribution and homogeneous lithic composition. The assumed seismic activity could still have played an important role in triggering this and other megabed events, even when sediment overburden is implied.

Comparison with Sorbas Basin

Since the Tabernas basin was connected to the Sorbas basin to the east, comparison with the stratigraphy of this basin is compelling. The Sorbas basin contains one of the most complete sedimentary successions of Messinian age of the Mediterranean and is astronomically tuned (Krijgsman et al., 2001). Regrettably, the tuning and dating of older strata, such as the shallow marine calcarenites of the Azagador, has not been performed because of the lack of expression of precession induces cycles and the Late Tortonian unconformity at the base of the Azagador (Weijermars et al., 1985), hampering a good correlation to the East-West composite section.

In the Puente de Los Callejones section, the Messinian North section does not provide enough bio-events for a reliable correlation to the Sorbas basin stratigraphy. This correlation is more problematic due to missing coiling directions and abundance records of *G. scitula* in the Sorbas basin. While this correlation remains an enigma for now, so is a possible interconnection between the timing and origin of the Tabernas megabeds and the Sorbas thick shell-debris (TSB) as has been suggested by Puga-Bernabéu et al. (2007).

Future studies

Several interesting subjects for future study are suggested:

1) The biostratigraphic comparison of the Puente de Los Callejones section to the Monte del Casino section proved to be essential for obtaining reliable age constraints. Because the sedimentation rates in the Puente de Los Callejones section are much higher than for the Monte del Casino section, spacing between biostratigraphic events is higher, yielding less correlation points in sections of the same stratigraphic length. Especially for sections with remarkably high sedimentation rates, therefore spanning short time-intervals, it is important to obtain the highest possible number of age calibration points in order to reliably date events (the MBs) and assess sedimentation rates. The quality of the foraminiferal yield in the studied section is not as good as for other Mediterranean sections, yet there is some room for improvement in the methodology by introducing a second sieving step (after density separation). If the age of especially the coiling changes of *G. scitula* and possible morphological variations could be improved in astronomically tuned sections (preferably according to the ATNTS2012), the biostratigraphy of turbiditic sediments with high sedimentation rates can be dated more accurately, further constraining the age of the megabeds.

2) Previous study has shown water depth in the Tabernas basin to be around 600m during the Late Tortonian (Kleverlaan, 1989a), based on unpublished results of planktonic to benthic foraminiferal ratios. Using the biostratigraphic samples of the Puente de Los Callejones section, a more accurate reconstruction of water-depth can be made for the whole sampled interval, with improved planktonic to benthic foraminiferal ratio's (van der Zwaan et al., 1990) by correcting for in-benthic foraminiferal species.

3) North-west of the town Tabernas, Rogerson et al. (2006) have shown that study of benthic foraminiferal assemblages can distinguish the environment (slope, canyon, fan) at the time of deposition, providing a possible extra method for determining environmental changes in comparable sections, such as the Puente de Los Callejones section.

4) Relatively close to our section (to the West), another study focussed on transgressional/regressional cycles in a Gilbert-style delta system (García-García et al., 2006), also assumed to be of Late Tortonian age, showing promising correlations of interpreted sealevel to the eustatic global sealevel curve (Haq et al., 1988) as well as more information on tectonic subsidence. Further constraints on tectonic subsidence, ultimately compared to the amount and timing of subsidence in the Alfaro sub-basin, would greatly enhance our understanding of the history of the basin.

Conclusions

We successfully established a detailed lithostratigraphy, biostratigraphy and magnetostratigraphy for a 730 m succession of turbiditic sediments in the Tabernas basin, unfortunately the two resulting composite sections are separated by a large stratigraphic gap (in a fault zone) covering between 98 to 253 kyr and including the Tortonian/Messinian boundary. The results confirm that the turbiditic sediments and megabed 1, 3 and the Gordo Megabed (GMB/MB2) in the East-West composite section are of Late

Tortonian age, while megabeds 4 to 7 located in the North section are of Early Messinian age.

More accurate ages of the megabeds are calculated based on linear interpolation of sedimentation rates with best estimates yielding ages of: MB1) 7.411 ± 0.003; GMB) 7.375 ± 0.018; MB3) 7.358 ± 0.005; MB4) 7.060 ± 0.013; MB5) 7.031 ± 0.009; MB6) 6.963 ± 0.016; MB7) 6.930 ± 0.022 Ma (Table 3).

The transition of stratigraphic Unit C to D (as defined by Haughton) is dated at about 7.515 Ma in the studied section. Sedimentation rates vary considerably throughout the East-West section, with the oldest studied sediments (lower ~100 m) having lower sedimentation rates of 0.52-1.78 m/kyr than the rest of the section with 2.9-3.2 m/kyr.

The megabeds in the North section are exposed in a continuous ridge with clear difference in erosional profile, with megabeds located in more pronounced turbiditic sequences.

We propose that the importance of sediment overburden or availability of sediments should be re-validated as a possible factor for megabed deposition, since the megabeds: 1) share a sheetlike deposition style; 2) are all single event mass-flows; 3) are more common in the stratigraphic record then previously thought; 4) the system supplying mass-flow material might have been active for a long time; 5) seem to coincide with periods of increased thickness (relief) and frequency of turbidites (in the North section). Possibly this overburden or sediment availability might be caused by climate cyclicity (precipitation and run-off).

On average, sedimentation rates in the basin were an order of magnitude higher than in the adjacent Sorbas basin. The megabeds in the Tabernas basin can not readily be linked to the Sorbas thick shell-debris (TSB) layers because accurate dating is missing for the TSB layers and inferred ages for the Tabernas megabeds are of too low resolution, however, we still consider a correlation plausible.

For best biostratigraphic correlations of sections with high sedimentation rates (such as the Puente de Los Callejones section), a higher density of accurately dated (astronomically tuned) biostratigraphic markers is required. We recommend to improve the accuracy of especially the coiling changes of *G. scitula* and possible morphological variations in astronomically tuned sections (preferably according to the ATNTS2012). Subsequently the biostratigraphy of the turbiditic sediments can be dated more accurately, further constraining the age of the megabeds.

Acknowledgments

We gratefully thank MSc A. Slootman and MSc. J. Verbaas for their strenuous efforts during the 5 week field campaign in the hot summer of 2011 and their geological and personal insights, being on fieldwork with them is always a joy. We thank Dr. Peter Haughton for his inspiring thoughts during the fieldwork and Niels de Winter for taking photographs of the section. Suggestions and constructive comments by Frits Hilgen and Wout Krijgsman were greatly appreciated, which lead to a significant improvement of the manuscript. This study was in part financially supported by Stichting Molengraaff Fonds (STMF), TU Delft.

References

Anson, G.L., Kodama, K.P., 1987. Compaction-induced inclination shallowing of the postdepositional remanent magnetization in a synthetic sediment. Geophysical Journal of the Royal Astronomical Society 88, 673–692.

Berggren, W.A., Kent, D.V., Couvering, J.A., 1985. The Neogene: Part 2 Neogene geochronology and chronostratigraphy. Geological Society Memoir 10, 211–260.

Bouma, A.H., 1962. Sedimentology of some Flysch deposits: A graphic approach to facies interpretation. Elsevier B.V.

Deamer, G.A., Kodama, K.P., 1990. Compaction-induced inclination shallowing in synthetic and natural clay-rich sediments. Journal of Geophysical Research 95, 4511–4529.

Dupont-Nivet, G., Krijgsman, W., 2012. Magnetostratigraphic methods and applications, in: Busby, C., Azor, A. (Eds.), Tectonics of Sedimentary Basins: Recent Advances. Blackwell Publishing Ltd., pp. 80–94.

García-García, F., Fernández, J., Viseras, C., Soria, J.M., 2006. High frequency cyclicity in a vertical alternation of Gilbert-type deltas and carbonate bioconstructions in the late Tortonian, Tabernas Basin, Southern Spain. Sedimentary Geology 192, 123–139.

Haq, B.U., Hardenbol, J., Vail, P.R., 1988. Mesozoic and Cenozoic chronostratigraphy and cycles of sea-level change, in: Wilgus, C.K., Hastings, B.S., Kendal, C.G.S.C., Posamentier, H., Ross, C.A., Van Vagoner, J.C. (Eds.), Sea-level Changes: An Integrated Approach. Society of Economic Paleontologists and Mineralogists, pp. 71–108.

Haughton, P.D.W., 2000. Evolving turbidite systems on a deforming basin floor, Tabernas, SE Spain. Sedimentology 47, 497–518.

Haughton, P.D.W., 2001. Contained turbidites used to track sea bed deformation and basin migration, Sorbas Basin, south-east Spain. Basin Research 13, 117–139.

Hilgen, F.J., Krijgsman, W., Langereis, C.G., Lourens, L.J., Santarelli, a., Zachariasse, W.J., 1995. Extending the astronomical (polarity) time scale into the Miocene. Earth and Planetary Science Letters 136, 495–510.

Hodgson, D.M., Haughton, P.D.W., 2004. Impact of syndepositional faulting on gravity current behaviour and deep-water stratigraphy: Tabernas-Sorbas Basin, SE Spain. Geological Society, London, Special Publications 222, 135–158.

Hüsing, S.K., Kuiper, K.F., Link, W., Hilgen, F.J., Krijgsman, W., 2009. The upper Tortonian–lower Messinian at Monte dei Corvi (Northern Apennines, Italy): Completing a Mediterranean reference section for the Tortonian Stage. Earth and Planetary Science Letters 282, 140–157.

Iaccarino, S., 1975. Litostratigrafia e biostratigrafia di alcune serie neogeniche della provincia di Almeria (Andalusia orientale - Spagne). Ateneo Par- mense, Ada Nat. 11, 237–313.

Iosifidi, A.G., Mac Niocaill, C., Khramov, A.N., Dekkers, M.J., Popov, V.V., 2010. Palaeogeographic implications of differential inclination shallowing in permo-carboniferous sediments from the donets basin, Ukraine. Tectonophysics 490, 229–240.

Kirschvink, J.L., 1980. The least-squares line and plane and the analysis of palaeomagnetic data. Geophysical Journal, Royal Astronomical Society 62, 699–718.

Kleverlaan, K., 1987. Gordo Megabed; A possible seismite in a Tortonian submarine fan, Tabernas basin, Province Almeria, Southeast Spain. Sedimentary Geology 51, 165–180.

Kleverlaan, K., 1989a. Neogene history of the Tabernas basin (SE Spain) and its Tortonian submarine fan development. Geologie en Mijnbouw 68, 421–432.

Kleverlaan, K., 1989b. Three distinctive feeder-lobe systems within one time slice of the Tortonian Tabernas fan, SE Spain. Sedimentology 36, 25–45.

Krijgsman, W., Fortuin, a. R., Hilgen, F.J., Sierro, F.J., 2001. Astrochronology for the Messinian Sorbas basin (SE Spain) and orbital (precessional) forcing for evaporite cyclicity. Sedimentary Geology 140, 43–60.

Krijgsman, W., Garces, M., 2004. Palaeomagnetic constraints on the geodynamic evolution of the Gibraltar Arc. Terra Nova 16, 281–287.

Krijgsman, W., Hilgen, F.J., Negri, A., Wijbrans, J.R., Zachariasse, W.J., 1997. The Monte del Casino section (Northern Apennines, Italy): a potential Tortonian/Messinian boundary stratotype? Palaeogeography, Palaeoclimatology, Palaeoecology 133, 27–47.

De Lamotte, D.F., Guezou, J.-C., Averbuch, O., 1995. Distinguishing lateral folds in thrust-systems; examples from Corbières (SW France) and Betic Cordilleras (SE Spain). Journal of Structural Geology 17, 233–244.

Laskar, J., Robutel, P., Joutel, F., Gastineau, M., Correia, A.C.M., Levrard, B., 2004. A long-term numerical solution for the insolation quantities of the Earth. Astronomy & Astrophysics 428, 261–285.

Lourens, L.J., Hilgen, F.J., Shackleton, N.J., Laskar, J., Wilson, J., 2004. Appendix 2. Orbital tuning calibrations and conversions for the Neogene Period, in: Gradstein, F.., Ogg, J.G., Smith, A.G. (Eds.), A Geologic Time Scale 2004. Cambridge University Press, Cambridge, U.K., pp. 469–471.

Meijninger, B.M.L., Vissers, R.L.M., 2006. Miocene extensional basin development in the Betic Cordillera, SE Spain revealed through analysis of the Alhama de Murcia and Crevillente Faults. Basin Research 18, 547–571.

Montenat, C., Ott d'Estevou, P., Masse, P., 1987. Tectonic- sedimentary characters of the Betic Neogene basins evolving in a crustal transcurrent shear zone (SE Spain). Bulletin - Centres de Recherches Exploration-Production Elf- Aquitaine 11, 1–22.

Platt, J.P., Vissers, R.L.M., 1989. Extensional collapse of thickened continental lithosphere: A working hypothesis for the Alboran Sea and Gibraltar arc. Geology 17, 540–543.

Poisson, A.M., Morel, J.L., Andrieux, J., Coulon, M., Wernli, R., Guernet, C., 1999. The origin and development of Neogene basins in the Betic Cordillera (SE Spain): A case study of the Tabernas-Sorbas and Huercal Overa basins. Journal of Petroleum Geology 22, 97–114.

Postma, G., Hilgen, F.J., Zachariasse, W.J., 1993. Precession-puntuated growth of a late Miocene submarine-fan lobe on Gavdos (Greece). Terra Nova 5, 438–444.

Puga-Bernabéu, Á., Martín, J.M., Braga, J.C., 2007. Tsunami-related deposits in temperate carbonate ramps, Sorbas Basin, southern Spain. Sedimentary Geology 199, 107–127.

Rio, D., Raffi, I., Villa, G., 1990. Pliocene-Pleistocene calcareous nannofossil distribution patterns in the western Mediterranean. Proceedings of the Ocean Drilling program, Scientific Results 107, 513–533.

Robinson, P., Harrison, R.J., Mcenroe, S.A., Hargraves, R.B., 2002. Lamellar magnetism in the haematite – ilmenite series as an explanation for strong remanent magnetization. Nature 418, 517–520.

Rogerson, M., Kouwenhoven, T.J., van der Zwaan, G.J., O'Neill, B.J., van der Zwan, C.J., Postma, G., Kleverlaan, K., Tijbosch, H., 2006. Benthic foraminifera of a Miocene canyon and fan. Marine Micropaleontology 60, 295–318.

Semensatto Jr, D.L., Dias-Brito, D., 2007. Alternative saline solutions to float foraminiferal tests. Journal of Foraminiferal Research 37, 265–269.

Sierro, F.J., Hilgen, F.J., Krijgsman, W., Flores, J. a., 2001. The Abad composite (SE Spain): a Messinian reference section for the Mediterranean and the APTS. Palaeogeography, Palaeoclimatology, Palaeoecology 168, 141–169.

Vissers, R.L.M., Platt, J.P., van der Wal, D., 1995. Late orogenic extension of the Betic Cordillera and the Alboran Domain: A lithospheric view. Tectonics 14, 786–803.

Weijermars, R., Roep, T.B., Eeckhout, B. van den, Postma, G., Kleverlaan, K., 1985. Uplift history of a Betic fold nappe inferred from Neogene-Quaternary sedimentation and tectonics (in the Sierra Alhamilla and Almeria, Sorbas and Tabernas Basins of the Betic Cordilleras, SE Spain). Geologie en Mijnbouw 64, 397–411.

Zijderveld, J.D.A., 1967. A.C. demagnetization of rocks: analysis of results. In: Developments of Solid Earth Geosciences Methods in Paleomagnetism. Elsevier Publishing Company, Amsterdam.

van der Zwaan, G.., Jorissen, F.., de Stigter, H.., 1990. The depth dependency of planktonic/benthic foraminiferal ratios: Constraints and applications. Marine Geology 95, 1–16.